ELSEVIER

Journal of Fluids and Structures 25 (2009) 697–712

JOURNAL OF FLUIDS AND STRUCTURES

www.elsevier.com/locate/jfs

Fluid forcing, wake modes, and transitions for a cylinder undergoing controlled oscillations

T.L. Morse, C.H.K. Williamson*

Sibley School of Mechanical and Aerospace Engineering, Upson Hall, Cornell University, Ithaca, NY 14853, USA

Received 6 June 2008; accepted 12 December 2008
Available online 5 April 2009

Abstract

In this study, we make extensive measurements of the fluid forces on a cylinder that is controlled to oscillate transverse to a free stream at $Re = 4000$. These measurements are used to create very high resolution contour plots (considerably higher than in any previous study) of the magnitude of fluid forcing, and its phase relative to the cylinder motion (as well as other fluid forcing quantities) in the plane of normalized amplitude and wavelength. Previous contours of force have been assumed to be continuous in the amplitude–wavelength plane, despite the fact that jumps in the fluid forcing and vortex formation modes were known to occur in other studies, including free vibration. In this investigation, we find clear discontinuities in the force contours, and we are thus able to identify boundaries separating different fluid forcing regimes. These appear remarkably similar to boundaries separating different vortex shedding modes in the regime map of Williamson and Roshko [1988. Vortex formation in the wake of an oscillating cylinder. Journal of Fluids and Structures 2, 355–381]. Measurements of vorticity fields confirm the modes of vortex formation in each regime; we find the 2S, 2P, and P + S modes, as well as a regime where the vortex formation is not synchronized with the cylinder oscillation. A new characteristic, which is only observable with very high-resolution data, is the existence of a region where two vortex formation regimes overlap. In the overlap region, we identify a distinct mode of vortex formation where two pairs of vortices are shed per cycle of oscillation (similar to the 2P mode) but the secondary vortex is much weaker, which we have termed '$2P_{OVERLAP}$', or simply the '$2P_O$' mode. The wake can switch intermittently between the 2P and $2P_O$ modes, even as the cylinder is oscillating with constant amplitude and frequency. The highest amplitude yielding positive fluid excitation lies inside the overlap region, therefore a study of the vortex dynamics in this region is essential to understanding the behavior of a free vibration system at peak amplitude response.

Keywords: Oscillating cylinder; Vortex formation modes; Vortex-induced vibration

1. Introduction

Much of the interest in the flow around a cylindrical body oscillating transversely to a free stream is due to its relevance to vortex-induced vibration, which occurs when a body is placed in a flow and the fluctuating lift force due the asymmetric formation of vortices in the wake causes the body to vibrate. Vortex-induced vibration is an important problem in many fields of engineering, affecting the dynamics of riser tubes bringing oil from the seabed to the surface, as well as civil engineering structures such as bridges, chimneys, and buildings, among other applications. The range of

*Corresponding author. Tel.: +1 607 255 9115; fax: +1 607 255 1222.
E-mail address: cw26@cornell.edu (C.H.K. Williamson).

0889-9746/$ - see front matter
doi:10.1016/j.jfluidstructs.2008.12.003

Table 1
Non-dimensional groups.

Normalized wavelength	λ^*	$\frac{\lambda}{D}=\frac{U}{fD}$
Normalized amplitude	A^*	$\frac{A}{D}$
Transverse force coefficient	C_Y	$\frac{F_Y}{\frac{1}{2}\rho U^2 DL}$
Reynolds number	Re	$\frac{\rho UD}{\mu}$

In the above groups, U is the free-stream velocity, λ is the oscillation wavelength, f is the oscillation frequency, D is the cylinder diameter, L is the submerged cylinder length, v is the fluid kinematic viscosity, ρ is the fluid density, and F_Y is the transverse fluid force.

problems caused by vortex-induced vibration has led to a large number of experimental and computational studies on the subject, including several review articles, for example Sarpkaya (1979), Griffin and Ramberg (1982), Bearman (1984), Parkinson (1989), and Williamson and Govardhan (2004).

In the present study, we are interested in the fluid forcing and wake modes that arise from controlled vibration, where a cylinder is prescribed to move with a sinusoidal motion transverse to a free stream. For such a motion, the relevant parameters, in addition to Reynolds number (Re), are the oscillation amplitude (A), and the oscillation wavelength (λ), or the oscillation frequency (f), which in this study we nondimensionalize as shown in Table 1. The normalized wavelength, $\lambda^* = \lambda/D = U/fD$ is equivalent to the ratio U^*/f^* used in free vibration studies such as Govardhan and Williamson (2000) where $U^* = U/f_N D$, $f^* = f/f_N$ with f_N being the natural frequency of the structure. The normalized wavelength may also be multiplied by the Strouhal number (S) to obtain the ratio of the stationary cylinder shedding frequency (f_{vo}) to the actual oscillation frequency (f), i.e. $\lambda^* S = f_{vo}/f$. In the present study, the Strouhal number was found to be 0.207.

The measured transverse force is often approximated by a sinusoidal function, thus the motion and force is often represented by

$$y(t) = A\sin(\omega t), \tag{1}$$

$$F(t) = F_{Y0}\sin(\omega t + \phi). \tag{2}$$

For certain regions of the parameter space, the fluid forcing exhibits somewhat non-sinusoidal behavior. However, in general, we shall present the component of forcing that occurs at the fundamental (body oscillation) frequency, based on a Fourier series analysis. This is the most relevant component, because other frequency components will not yield a net contribution to the energy transfer between the fluid and the body. The transverse force coefficient (at the fundamental) can be decomposed into two components, one in phase with velocity, $C_Y \sin\phi$ (which yields the 'fluid excitation') and one in phase with acceleration, $C_Y \cos\phi$ (which yields the 'effective added mass'). The phase, ϕ, between the fluid forcing and cylinder motion is an extremely important parameter as it determines whether the fluid adds or removes energy from the system and thus whether free vibration is possible.

There are several existing classical studies on fluid forcing for a cylinder undergoing controlled vibration. In a pioneering study, Bishop and Hassan (1964) showed that as the frequency of cylinder oscillation increases, there is a simultaneous jump in the magnitude of the fluid force (C_Y) and its phase (ϕ), which occurs at an oscillation frequency close to the frequency of vortex shedding for a stationary cylinder. Subsequent controlled vibration studies, such as the measurements of force for particular broadly spaced values of amplitude (which we shall call 'amplitude cuts') by Mercier (1973), and Sarpkaya (1977) have also found sharp jumps in the fluid forcing near the natural vortex shedding frequency for a stationary cylinder. In the present work, one of our objectives is to identify precisely the location of this jump, and other such force jumps, *throughout the normalized amplitude–wavelength plane* using our extremely high-resolution force data.

In order to make predictions of the response of an elastically mounted cylinder, Staubli (1983) generated contour plots of the lift force magnitude and phase angle from his controlled vibration force measurements. He compared his predictions to the free vibration measurements of Feng (1968), and found some regions of the response where the comparison is successful, and other regions where the comparison is not close. The most extensive force measurements to date come from Gopalkrishnan (1993), and Hover et al. (1998) who generated complete contour plots of the fluid forcing over a wide range of normalized amplitude and wavelength. The zero fluid excitation curve ($C_Y \sin\phi = 0$) obtained from these contours was shown in Hover et al. (1998) to have generally good agreement with a free vibration response at very low mass-damping (as one might expect), however some portions of the response lay in regions where the force data from controlled vibration predicted negative excitation.

One important question for these controlled vibration studies is to what extent can their results be applied to the case of a freely vibrating, elastically mounted cylinder. As mentioned above, and pointed out by Williamson and Govardhan (2004), as well as Carberry et al. (2004), several past controlled vibration studies have found negative fluid excitation for values of normalized amplitude and wavelength at which free vibration is known to occur, suggesting that controlled vibration results may not necessarily be used to predict accurately the free vibration case. However, Morse and Williamson (2006) made direct comparisons between free and controlled vibration and showed that *if the experimental conditions are carefully matched*, controlled vibration can yield fluid forces which are in very close agreement with results from free vibration, over an entire response plot.

In addition to these force measurements, there have been several studies focusing on the wake of an oscillating cylinder. Ongoren and Rockwell (1988a) examined the near wake of an oscillating circular cylinder as well as several other body geometries and found that there is a switch in timing of the vortex formation across the phase jump found by Bishop and Hassan (1964). Williamson and Roshko (1988) conducted an extensive study of the different vortex shedding modes that exist for an oscillating cylinder, which they defined, for example as a '2S' mode indicating two single vortices formed per cycle, a '2P' mode meaning two pair of vortices formed per cycle, and an asymmetric 'P + S' mode comprising a pair of vortices and a single vortex per cycle. They mapped out where these modes occur in the plane of normalized amplitude and wavelength as may be seen later in Fig. 3(b). Ongoren and Rockwell (1988b) observed patterns similar to the 2S, 2P, and P + S modes for the case of a cylinder oscillating in-line with the flow.

Carberry et al. (2001) made simultaneous force and wake vorticity measurements in controlled vibration. They showed that the well-known jump in fluid forcing described above was due to a change in vortex formation pattern from the 2P to the 2S mode, which is consistent with the free vibration results of Govardhan and Williamson (2000). This transition was further characterized with various chosen 'amplitude cuts' and Reynolds numbers in Carberry et al. (2005). They found that at frequencies (f) near the (stationary cylinder) shedding frequency (f_{vo}), the vortex shedding mode depended on the initial conditions and in fact, for a certain band of frequencies, the wake could make a one-time transition from one mode to the other, even while the frequency was held constant. Pottebaum (2003) conducted experiments on heated cylinders oscillating in a flow and found that, in certain regimes, the wake could switch intermittently between the 2S and 2P modes. He concluded that this phenomenon was likely due to temperature induced variations in the fluid viscosity. In the present study, we will show regions where the wake switches intermittently between vortex formation modes, in the absence of any temperature variations.

In this work, we conduct controlled vibration experiments over an extensive range of normalized amplitude and wavelength with very high resolution, much higher than in any previous data set, as shown in Fig. 1, amounting to 5680 experimental runs, each of which comprises 100 cycles of oscillation. One of the original motivations for the force data presented here was to obtain very high resolution force contours using precisely the same flow facility and experimental arrangement as in Govardhan and Williamson (2000, 2006), in order to make accurate predictions of the free vibration response. Comprehensive analysis and further extensive measurements linking controlled vibration with free vibration response will be presented in Morse and Williamson (2009). In the present paper, we focus on defining the regimes of vortex shedding and especially on the transitions between these regimes.

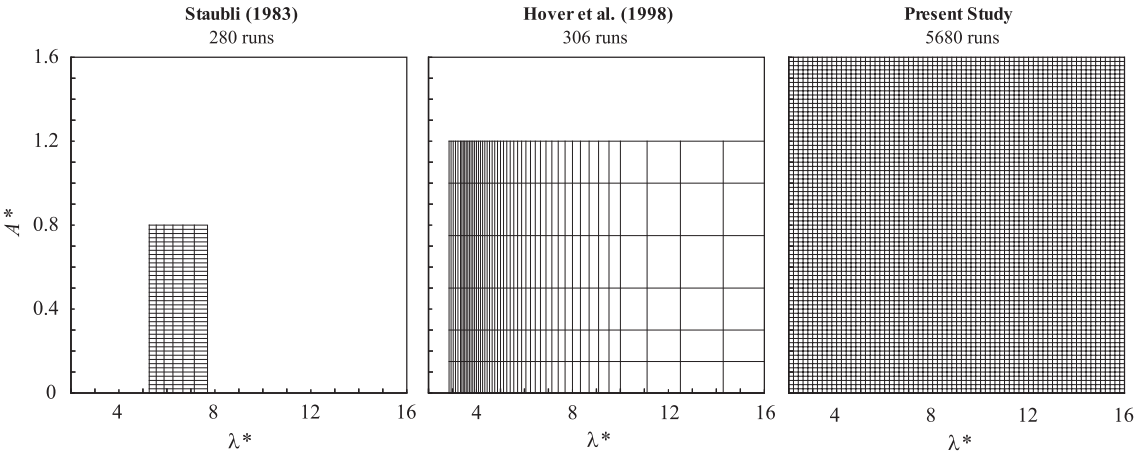

Fig. 1. Grid resolution of controlled vibration measurements from the previous studies and in the present study. We are able to obtain a very high resolution, as well as a wide range of the parameters.

Following a description of the experimental details in Section 2, we show contours of fluid forcing obtained from our high resolution data in Section 3. Boundaries between vortex shedding modes are determined by looking for abrupt jumps in the character of the fluid forcing. We also present DPIV measurements of the vorticity for these different modes. In Section 4 we characterize the mode boundaries by looking more closely at time traces of the fluid forcing. This is followed by the conclusions in Section 5.

2. Experimental details

The present experiments are conducted in the Cornell-ONR Water Channel, which has a cross-section of 38.1 cm × 50.8 cm. The turbulence level in the test section of the water channel is less than 0.9%. A cylinder of diameter 3.81 cm and length 38.1 cm is suspended vertically in the water channel and forced to oscillate transverse to the flow using a computer-controlled motor attached to a transverse lead screw, as shown schematically in Fig. 2. The flow speed is kept constant to give $Re = 4000$. A fixed end plate is placed 2 mm below the bottom of the cylinder (but not in contact with the cylinder) to encourage two-dimensional vortex shedding, following the study of Khalak and Williamson (1996). A total of 5680 runs, each for 100 cycles of oscillation, are conducted for approximately 500 hours worth of data. Normalized amplitude (A^*) is varied from 0.02 to 1.6 with a resolution of 0.02. Normalized wavelength (λ^*) is varied from 2 to 16 with a resolution of 0.2. Such an extensive data set is only possible because the experiment is conducted in a continuously flowing water channel facility, and thus can be automated to run unattended for a large number of experimental runs.

A two-axis force balance utilizing linear variable distance transducers (LVDTs) is used to measure the lift and drag forces on the cylinder. The transverse displacement of the cylinder is measured using a non-contact (magnetostrictive) position transducer. For each run, the fluid force magnitude and phase angle (relative to the body motion) at the fundamental (body oscillation) frequency is calculated using a Fourier series analysis. In most cases, the fluid forcing is quite sinusoidal and thus the component at the fundamental frequency represents essentially all of the force signal content. In some cases, which are discussed in Section 4.3 (for example in the desynchronized regime), the fluid forcing is less sinusoidal, and the component at the fundamental may represent only a small portion of the total force signal content.

In addition to the extensive force measurements described above, we also use digital particle image velocimetry (DPIV) to examine the cylinder wake. The flow is seeded with 14-micron silver coated glass spheres, which are

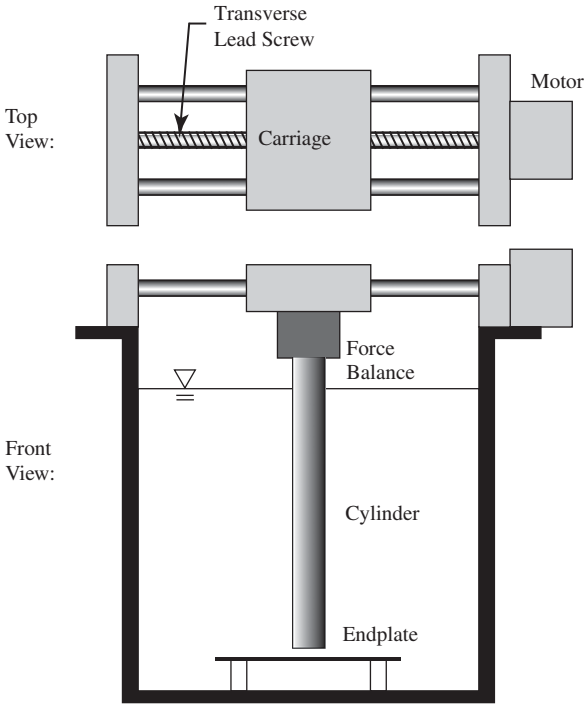

Fig. 2. Schematic diagram of the experimental arrangement. The cylinder is suspended vertically in a water channel and is oscillated transverse to the flow (into the page) using a computer controlled motor and lead screw.

illuminated by a sheet of laser light from a 50 mJ Nd:Yag pulsed laser. Pairs of particle images are acquired using a Jai CV-M2CL CCD camera (1600 × 1200 pixels), and analyzed using cross-correlation of sub-images. We use a two-step windowing process (with window shifting) to obtain particle displacements between image pairs. The viewing area is 26 cm × 34 cm corresponding to 6.75 by 9 diameters. The time between images is adjusted to vary between 10 and 20 ms depending on the cylinder oscillation parameters. Vorticity fields calculated from the image pairs are phase averaged over approximately 20 cycles to remove the smaller weak structures resulting from intermittent small-scale three-dimensionality in the flow and thus obtain a clear picture of the dynamics of the principal spanwise vorticity.

3. Fluid forcing contours and vortex formation modes

Upon examining our controlled vibration data, we notice that the fluid forcing shows qualitative abrupt jumps in certain regions as amplitude or frequency is varied. By following these jumps throughout the normalized amplitude–wavelength plane, we are able to identify clear boundaries separating regions of distinct fluid forcing, indicated by the colored regimes in Fig. 3(a). When these boundaries are compared to the boundaries separating different vortex formation modes in the Williamson and Roshko (1988) map in (b), we see a remarkable similarity. Thus we expect that the regions we identify, based solely on the fluid forcing, will correspond with different modes of vortex formation, similar to those of Williamson and Roshko.

One of the most interesting features of the map of regimes in Fig. 3 is the existence of regions where two modes overlap. In these overlap regions, the fluid forcing switches intermittently between two distinct modes even as the cylinder is oscillating with constant amplitude and frequency. This phenomenon appears in two places: as an overlap between the 2P region and the region where the wake is desynchronized (right hand edge of the yellow 2P region in Fig. 3), and more importantly, in a region that lies in between the 2P and 2S modes and overlaps them both, which we label '$2P_{OVERLAP}$' or more simply '$2P_O$'. This overlap phenomenon is different from the one-time switch in forcing found by Carberry et al. (2005) which is related to the hysteresis found by Bishop and Hassan (1964). It is similar to the switching behavior Pottebaum (2003) found for his heated cylinders, although in this case no temperature variation is required. We emphasize here that the discovery of these overlapping regions is only possible because of the high resolution used in this study.

We now wish to study which vortex formation modes exist in the different regimes of Fig. 3(a). In Fig. 4 we confirm the existence of the P + S, 2S, and 2P modes in the regions we expect them. We were initially curious to see what mode of vortex formation exists in the overlap region, lying between the 2P and 2S modes. Would it resemble one mode or the other, or something in between? What we find is a variation of the 2P mode, namely the '$2P_O$' mode, where, although there are two pairs of vortices shed per cycle, the secondary vortex is much weaker and decays rapidly as the vortex pair moves downstream, as shown in Fig. 4(b). This $2P_O$ vortex formation mode is equivalent to the 'intermediate wake state' identified by Carberry et al. (2003) in one of their 'amplitude cuts', existing for a narrow band of frequencies. It is also equivalent to the '$2P_{upper}$' mode found by Govardhan and Williamson (2000) in the same region of the normalized amplitude–wavelength plane, in their case for the 'upper branch' of a free vibration response at very low mass-damping. (Their '$2P_{lower}$' mode found in the 'lower branch' of free vibration is equivalent to the pure 2P mode described here.)

We note that the identification of a distinct $2P_O$ mode would not be possible from free vibration experiments since the change in strength of the secondary vortex is accompanied by a change in amplitude of vibration, and we would thus interpret the two different modes as simply an amplitude effect changing the character of only one mode. Here we show that, even for constant amplitude and frequency, both the 2P and $2P_O$ modes can exist. From the vorticity field in Fig. 4(b) we see that one could easily mistake the $2P_O$ mode for a 2S mode depending on how well one resolved the small secondary vortex.

Now that we have defined the different regions of vortex formation, we plot precise, high-resolution contours of key fluid forcing parameters. Here we show contours of the force in phase with velocity, $C_Y \sin\phi$, and contours of the force in phase with acceleration, $C_Y \cos\phi$, shown in Fig. 5. Further contours of force and phase are included in Appendix A. It is not possible to plot *continuous* contours across our complete parameter space (as presented in some previous studies), due to the existence of overlapping modes and discontinuities, made evident from the resolution of the present data.

The force in phase with velocity, $C_Y \sin\phi$, represents a normalized 'fluid excitation', and thus determines in what regions free vibration may occur. From Fig. 5 we can see there exist positive excitation regions within the 2S, 2P, and desynchronized regimes. The P + S regime shows strongly negative fluid excitation, so we would not expect to see such a mode for a freely vibrating cylinder at this Re, and indeed no such free vibration response modes have been experimentally observed. The highest amplitude for which there is positive fluid excitation is inside the $2P_O$ region, thus a study of the fluid forcing and vortex dynamics in this region is key to understanding the dynamics of the cylinder at its peak amplitude of free vibration.

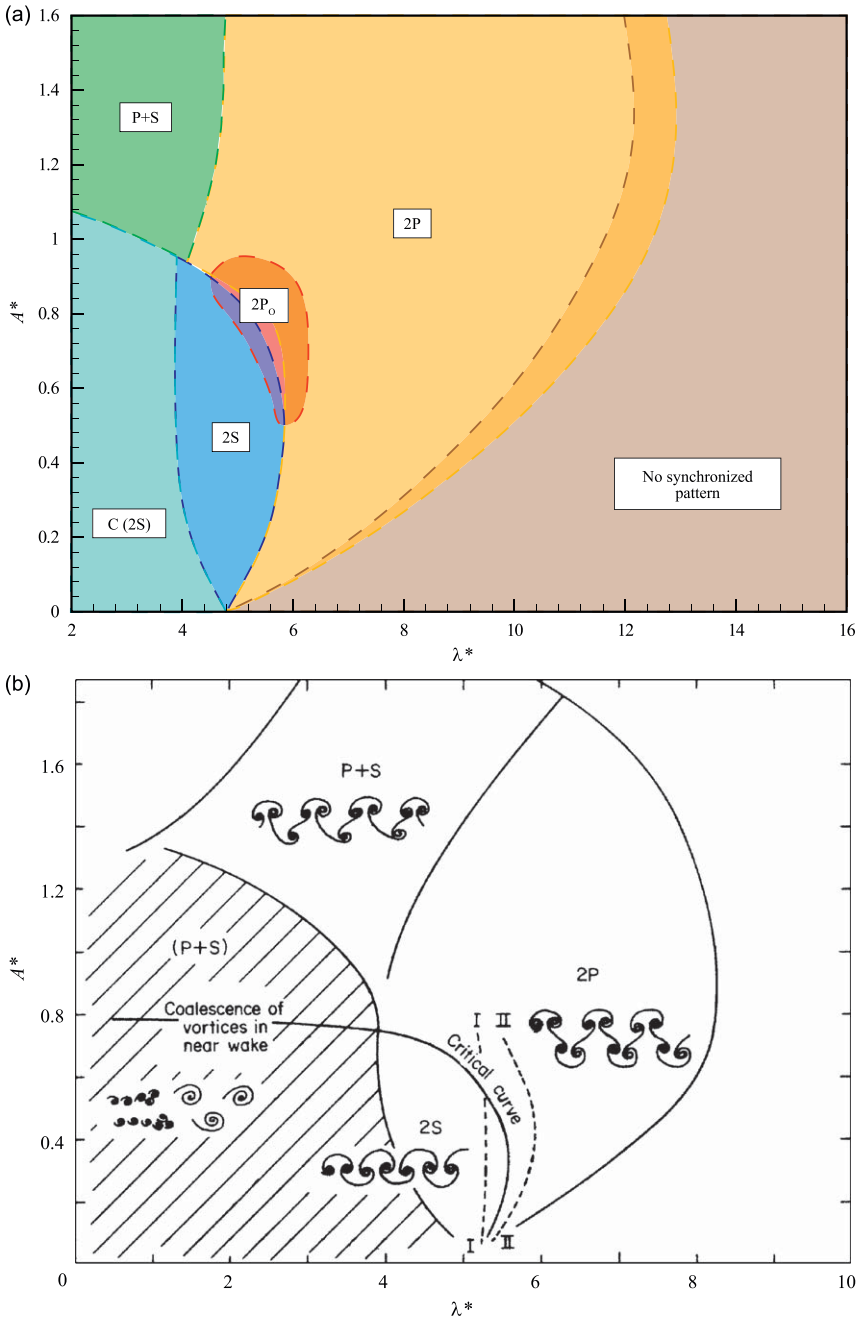

Fig. 3. Map of vortex shedding regimes. There is a remarkable similarity between (a) the mode boundaries we identify in the present study from force measurements and the (b) boundaries identified by Williamson and Roshko (1988) from flow visualization. Overlapping colors indicate regions where two vortex shedding modes overlap.

4. Characterizing wake mode boundaries and transitions

In the previous section, we identified different regimes of vortex formation in the normalized amplitude–wavelength plane. Although we used DPIV measurements of vorticity to verify the mode of vortex formation, the *boundaries defining these regimes were determined solely from the fluid forcing*. In this section we focus on time traces of the fluid

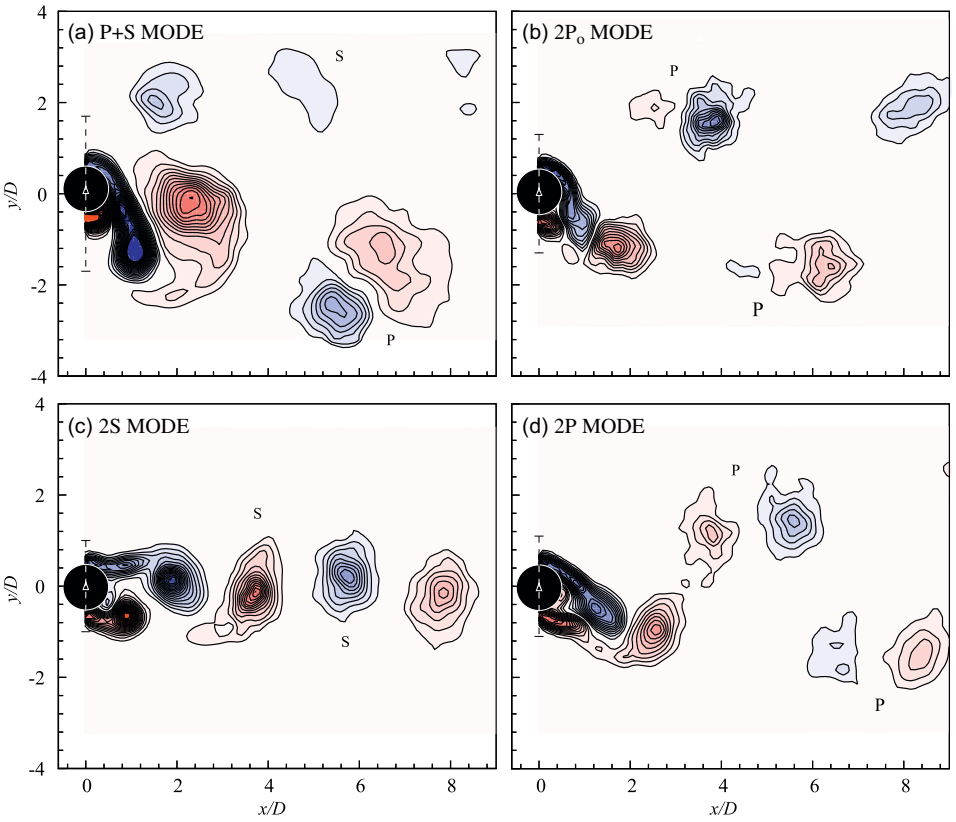

Fig. 4. Vorticity fields for each of the main vortex shedding modes P + S, 2S, 2P, and 2P$_O$. We observe a switch in timing of the initially shed vortex from the 2S mode to the 2P mode. In all cases the vorticity field is phase-averaged over 20 cycles of oscillation, contour levels shown are: $\omega D/U = \pm 0.4, \pm 0.8, \pm 1.2, \ldots$ Measurement locations are as follows: P + S mode: ($A^* = 1.2, \lambda^* = 4.0$); 2P$_O$ mode: ($A^* = 0.8, \lambda^* = 5.6$); 2S mode: ($A^* = 0.5, \lambda^* = 5.0$); 2P mode: ($A^* = 0.6, \lambda^* = 6.4$).

forcing across these boundaries, to characterize the nature of the transitions. The parameters defining these time traces are shown in Fig. 6, distinguished by the encircled numbers.

4.1. Mode boundaries with abrupt jumps in fluid forcing

In order to fully characterize the transition from the 2S to the 2P mode, it is necessary at this point to introduce the concept of the 'vortex force'. Following the analysis of Govardhan and Williamson (2000), we decompose the total transverse fluid force coefficient (C_{total}) into a 'potential force' component ($C_{\text{potential}}$) given by the potential added mass force, and a 'vortex force' component (C_{vortex}), due to the dynamics of vorticity. For sinusoidal body motion, the potential force coefficient can be calculated to be

$$C_{\text{potential}}(t) = 2\pi^3 \frac{y(t)/D}{(U^*/f^*)^2}. \tag{3}$$

Thus we see that the instantaneous potential added mass force, $C_{\text{potential}}$, is always in phase with the cylinder motion, $y(t)$, as one might expect. The vortex force coefficient can then be found by subtracting the potential force coefficient from the total force coefficient:

$$C_{\text{vortex}}(t) = C_{\text{total}}(t) - C_{\text{potential}}(t). \tag{4}$$

As a simplification of the nomenclature, we shall continue to use C_Y and ϕ to denote the magnitude and phase of the total force, and use C_V and ϕ_V to denote the magnitude and phase of the vortex force.

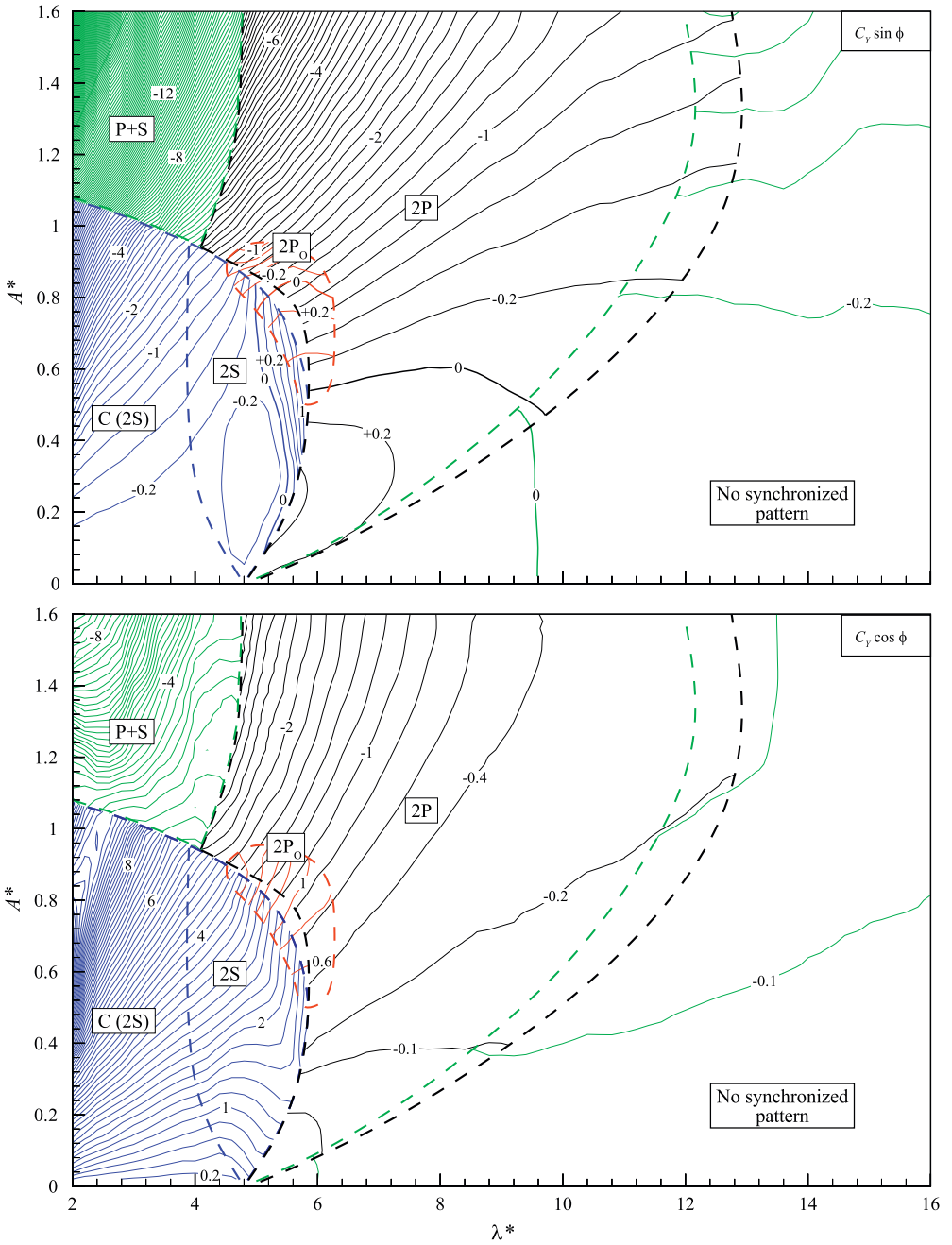

Fig. 5. Contours of the force in phase with velocity, $C_Y \sin\phi$ (normalized 'fluid excitation'), and the force in phase with acceleration, $C_Y \cos\phi$. Boundaries between modes are indicated by dashed lines. Note that contours overlap in regions where multiple vortex shedding modes are possible. Contour interval in both cases is 0.2 with an additional contour at $C_Y \cos\phi = -0.1$ for increased clarity.

The use of the concept of vortex force is useful to understand the transitions between the 2S and 2P modes because its variation more directly reflects changes in the vortex formation. The use of vortex force will be necessary to identify the $2P_O$ regime as described below.

The transition from the 2S to 2P mode of vortex formation at low amplitudes has been studied before. In the present work, we characterize the transition (see points 1 and 2 in Fig. 6) by looking at force time traces at similar values of normalized amplitude and wavelength on either side of the boundary, shown in Fig. 7. The magnitude of the vortex force is quite similar for both the 2S and 2P modes, however the vortex phase shows almost a 180° difference. This is

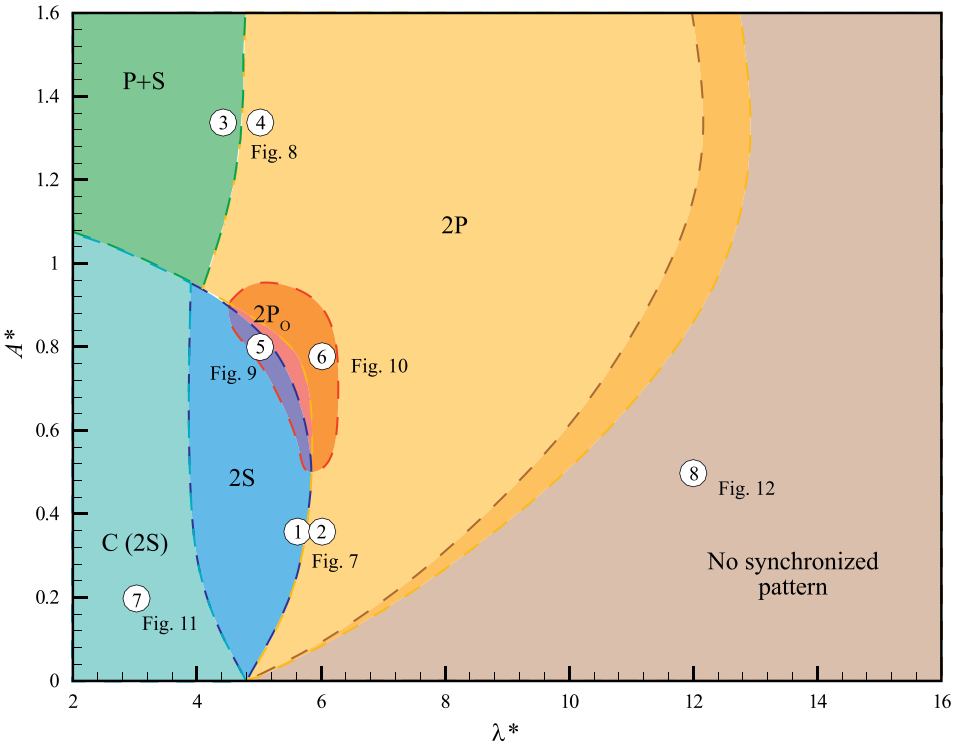

Fig. 6. Locations in the normalized amplitude–wavelength plane for which force time traces are shown in Figs. 7–12 (indicated by the encircled numbers).

due to the 180° switch in timing of the vortex formation as shown by the vorticity fields in Fig. 4 and identified by several previous investigations [for example Gu et al. (1994) and Govardhan and Williamson (2000)]. When the potential force, which has a phase of 0°, is added to the vortex force, the magnitude of the total force for the 2S mode becomes about four times greater than for the 2P mode, with a considerable phase jump also remaining.

In contrast to the 2S to 2P transition, for the P + S to 2P mode transition (points 3 and 4 in Fig. 6), neither the vortex force nor the total force show dramatic changes in magnitude or phase (although there is a small jump that may be seen in the contours of Figs. 13 and 14). Instead, the boundary between these modes is found by examining the shape of the fluid forcing time trace as in Fig. 8. For the P + S mode, the fluid forcing shows a clear asymmetry which can be further identified in the force spectra, with a strong peak in fluid forcing frequency (f_{FORCE}) at two times the oscillation frequency (f). With a small change in the normalized wavelength, the peak at $2f$ essentially vanishes, indicating a switch to the symmetric 2P mode of vortex formation (see Fig. 8). This change is abrupt, yielding a well-defined boundary.

4.2. Regimes of overlapping wake modes

For the boundaries described above, the transitions are abrupt with one clear vortex formation mode on either side of the boundary. We also find several regions where two distinct vortex formation modes can exist at a particular point in the (A^*, λ^*) plane. At these points, the forcing time trace reveals an intermittent switching in time between two distinct modes. For the case where the $2P_O$ mode overlaps with the 2S mode (point 5 in Fig. 6), this switching is most readily apparent in the vortex phase, as shown in Fig. 9. The vortex phase switches between a value near 0° and a value near 180°, corresponding with a switch in timing of the vortex formation as the wake transitions from the 2S mode to the $2P_O$ mode. In order to obtain the contours of the fluid forcing, in Fig. 5, the force signals were analyzed separately for each mode. We also point out that *if one were to look only at the total force, the different vortex formation modes could not be identified*, highlighting here the importance of using the vortex force formulation.

As we move through the $2P_O$ region we find a small sliver in the (A^*, λ^*) plane for which the $2P_O$ mode exists by itself (see Fig. 3). At slightly higher wavelength (point 6 in Fig. 6) there exists an overlap of the $2P_O$ mode and the standard 2P mode. Time traces of the fluid forcing, in Fig. 10, show that the vortex phase is near 180° for all times, indicating no

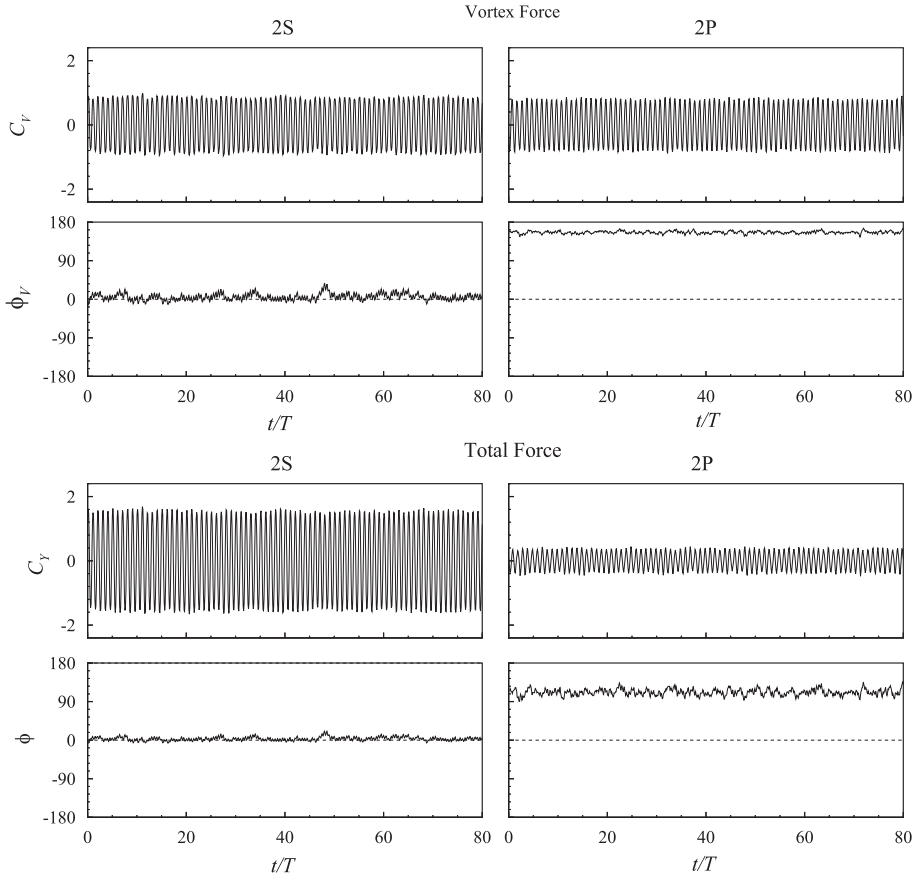

Fig. 7. Typical force time traces for the transition from the 2S mode to the 2P mode of vortex formation. The magnitude of the vortex force is nearly equal in both cases, however there is a large jump in the vortex phase, due to a change in the timing of vortex shedding. This difference in phase leads to a large difference in the magnitude of the total force. Time trace locations are points (1) and (2) in Fig. 6, 2S mode: ($A^* = 0.36, \lambda^* = 5.6$); 2P mode: ($A^* = 0.36, \lambda^* = 6.0$).

significant change in the timing of shed vortices. The switching becomes apparent when we look at the phase of the total force. When the wake is shedding vortices in the $2P_O$ mode, the magnitude of the vortex force is much smaller as compared to the pure 2P mode. Thus when the potential force (which always has a phase of 0°) is added back in, the total phase for the $2P_O$ becomes near 0°. Note that the inclusion of the potential force has no bearing on the sign of energy transfer, because ($C_Y \sin\phi$) is exactly equivalent to ($C_V \sin\phi_V$). In general, we find that the period of intermittent switching appears to be on the order of 10 cycles of oscillation. We expect that the switching period would depend on various aspects of the experimental setup, including incoming turbulence and spanwise end conditions.

4.3. Wake modes with non-synchronized fluid forcing

In the above sections, we have focused on regions for which the vortex formation is synchronized with the body motion. We shall now discuss two regimes where much of the fluid force is not synchronized with the body vibration. In one case, we have short wavelength (λ^* is small), causing a synchronized 2S mode, but the small vortices coalesce in the near wake, forming large scale structures: the C(2S) mode in Fig. 3. In the second case, we have a long wavelength (λ^* is large), such that several vortices form in each half cycle of vibration: the desynchronized vortex formation mode in Fig. 3.

For short wavelength, $\lambda^* < 4$, and for amplitudes, $A^* < 1$, the cylinder sheds alternately signed small vortices as it oscillates (i.e. the 2S mode), but these small vortices coalesce into larger-scale structures further downstream. For this coalescing 2S mode, or 'C(2S)' mode in Fig. 3, we find a significant component to the fluid forcing at a frequency (f_{FORCE}) below the oscillation frequency (f) as shown in Fig. 11(a). Since the coalescence does not occur with the same

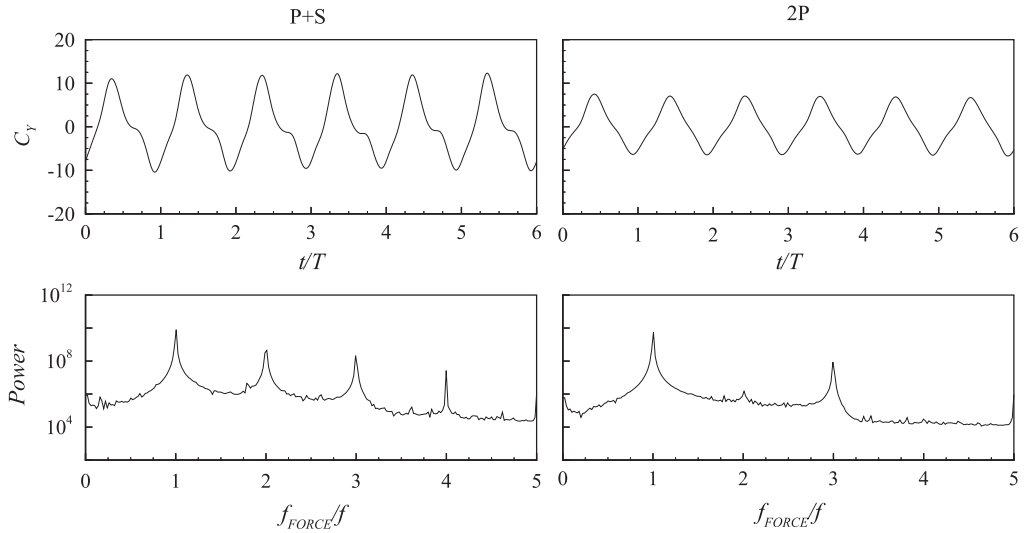

Fig. 8. Typical force time traces and spectra for the transition from the P + S mode to the 2P mode of vortex formation. The large peak at twice the oscillation frequency for the P + S mode is not found for the 2P mode. Locations are points (3) and (4) in Fig. 6, P + S mode: ($A^* = 1.34, \lambda^* = 4.4$); 2P mode: ($A^* = 1.34, \lambda^* = 5.0$).

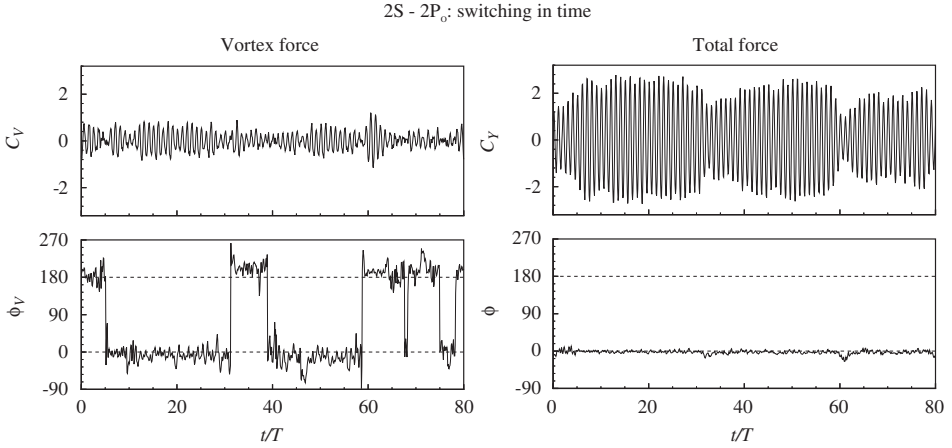

Fig. 9. Typical force time trace in the 2S−2P$_O$ region. The intermittent switching of the vortex formation mode is most apparent in the vortex phase, which jumps between a value close to 0° corresponding to the 2S mode, and a value close to 180° corresponding to the 2P$_O$ mode. Location is point (5) in Fig. 6: ($A^* = 0.8, \lambda^* = 5.0$).

timing for each cycle of vibration, the phase averaged vorticity field in (b) shows only weak structures downstream. Williamson and Roshko (1988), using flow visualization, showed that far downstream this coalescence could, under some conditions, lead to a vortex street of immense size, much larger than the scale of the oscillating body.

The boundary separating the C(2S) mode from the pure 2S mode is less distinct than any other boundary we identified. As the wavelength is increased, the low frequency forcing becomes smaller and smaller. We define the boundary in Fig. 3 as the point where the low frequency peak in the force spectra is no longer discernable.

At the high-wavelength end of the parameter space, beyond the 2P mode boundary in Fig. 3, we find a region where the transverse force time traces and spectra show forcing at a frequency (f_{FORCE}) higher than the oscillation frequency (f), as shown in the time traces of Fig. 12(a). In this case, we can think of the cylinder as moving through the fluid along an extended wavelength, shedding several vortices per half cycle. These vortices will not be synchronized with the motion, thus in the phase-averaged vorticity field of Fig. 12(b), no strong vorticity is found beyond a few diameters downstream. Note that even though the vortex shedding is desynchronized, there remains a distinct component to the fluid forcing at the oscillation frequency which, interestingly, would give rise to free vibration. Finally, for the narrow

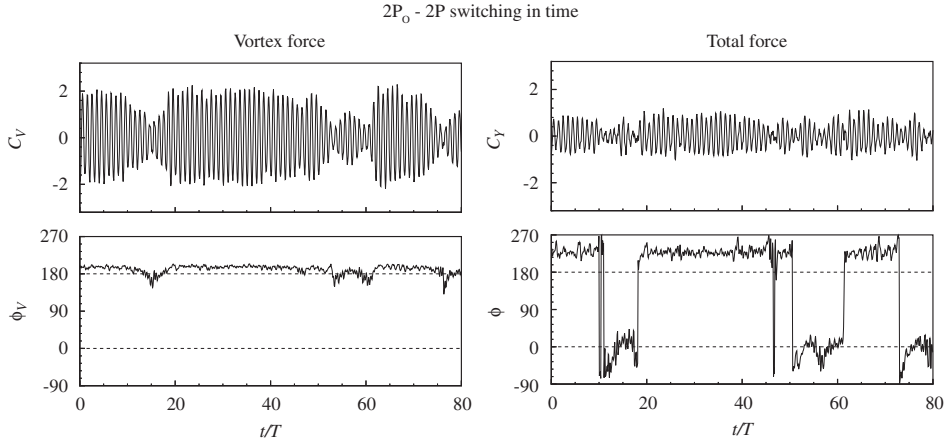

Fig. 10. Typical force time trace in the $2P_O-2P$ region. There is no dramatic change in vortex phase, however, the total phase reveals an intermittent switching between the two modes. For the pure 2P mode the phase is above 180° yielding negative excitation. For the $2P_O$ mode, the phase is near 0°. Location is point (6) in Fig. 6: ($A^* = 0.78, \lambda^* = 6$).

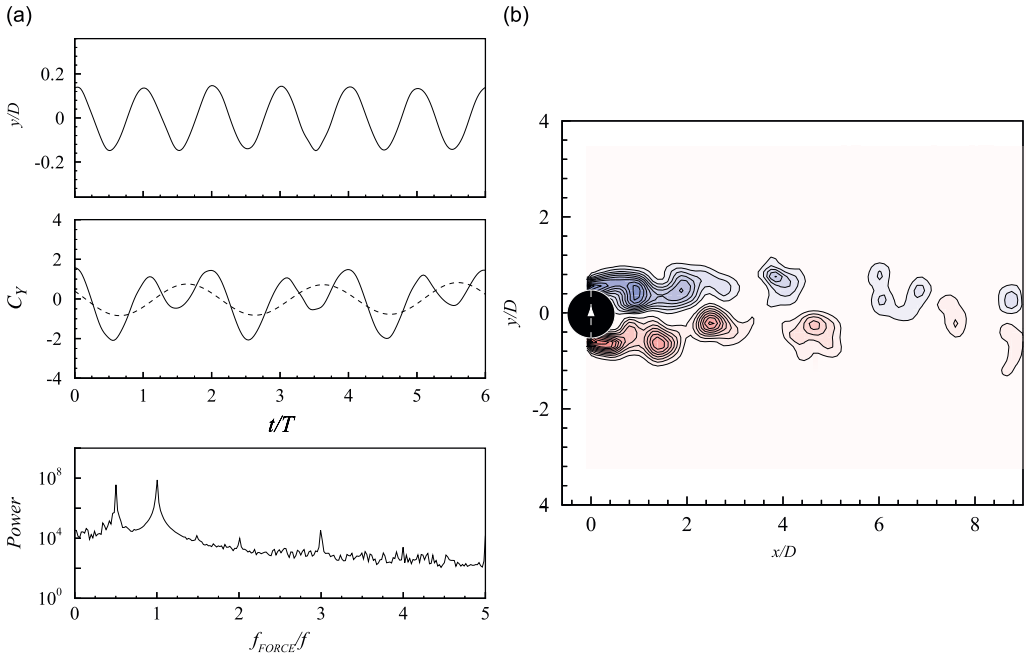

Fig. 11. The coalescing 2S mode of vortex formation: typical time traces, force spectra, and phase-averaged vorticity field. The dashed line in the force time trace shows only the component at the lower frequency which appears due to the coalescence of vortices downstream (the solid line shows the entire force signal). Contour levels shown for the vorticity field are: $\omega D/U = \pm 0.4, \pm 0.8, \pm 1.2, \ldots$ Location is point (7) in Fig. 6: ($A^* = 0.2, \lambda^* = 3$).

band of overlap between the 2P region and the desynchronized region, the fluid forcing switches intermittently in time between a synchronized single frequency forcing, and the type of desynchronized forcing shown in Fig. 12.

5. Conclusions

In this paper, we present new measurements of fluid force on a cylinder, whose controlled vibration is transverse to a flow, in the form of very high-resolution contour plots within the plane of normalized amplitude and wavelength

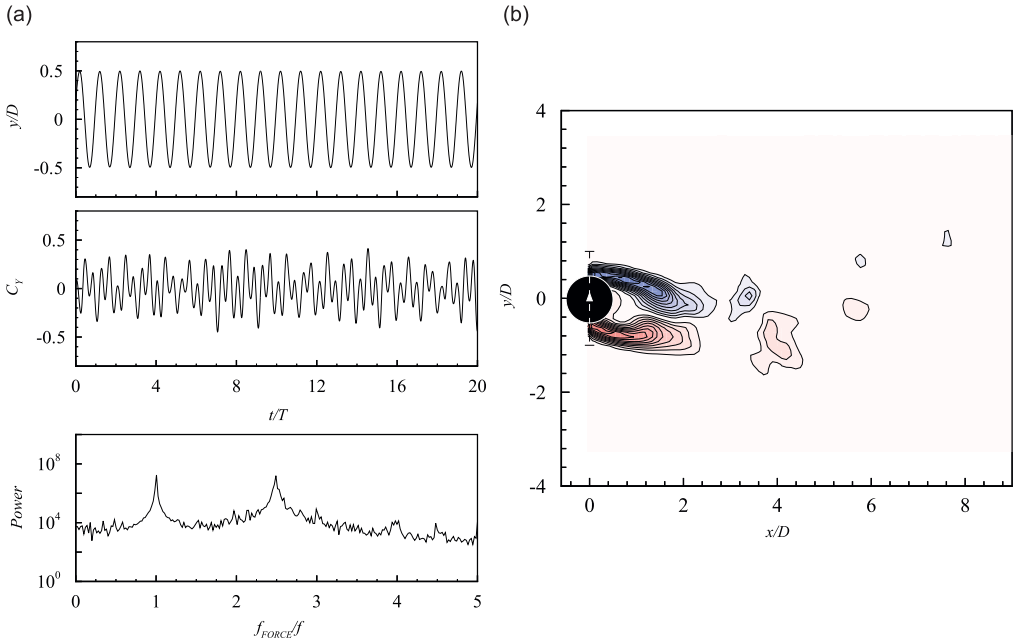

Fig. 12. Typical time traces, force spectra, and phase-averaged vorticity field in the desynchronized region. The fluid forcing is not synchronized with the cylinder motion, having a significant component near the natural vortex shedding frequency. Contour levels shown for the vorticity field are: $\omega D/U = \pm 0.4, \pm 0.8, \pm 1.2, \ldots$ Location is point (8) in Fig. 6: ($A^* = 0.5, \lambda^* = 12$).

(A^*, λ^*). Our principal contour diagrams comprise the force in phase with velocity ($C_Y \sin\phi$), which is also a normalized fluid excitation, and the force in phase with acceleration ($C_Y \cos\phi$), related to a normalized effective added mass. We include further contour plots of magnitude and phase of the total force (C_Y, ϕ) and of the vortex force (C_V, ϕ_V) in Appendix A.

In some previous studies, contour plots of fluid excitation in the plane of amplitude–wavelength have been assumed to be continuous, even though, on the basis of free vibration studies, as well as 'amplitude cuts' from controlled vibration studies, we expect that there must exist boundaries where vortex formation, and hence fluid force, would jump. However, our high resolution fluid excitation contours have made it possible to accurately determine several distinct boundaries, and to identify regimes in the plane of amplitude–wavelength, based solely on the force measurements. The contours are clearly *not continuous* across the whole range of amplitude–wavelength. Indeed, we find a remarkable agreement between the shapes of the regimes evaluated from force measurements, and the regimes of vortex formation modes identified from flow visualization found in the Williamson–Roshko (1988) map of regimes. By analyzing vortex modes in the present controlled vibration study using DPIV, we find the modes one would expect from comparison with the Williamson–Roshko map, namely the 2S and 2P modes, as well as the asymmetric P + S mode, which has been measured for the first time using DPIV in experiment.

The high resolution contour plots have further enabled us discover a new high-amplitude regime which overlaps the boundary between the 2S and 2P regimes. Vorticity measurements identify the new vortex formation mode to be one quite similar to the 2P mode, but where the second vortex of each pair is much weaker than the first vortex, in what we define as the '$2P_{OVERLAP}$' or '$2P_O$' mode. During an experiment, the vortex formation mode and fluid force switches intermittently between the $2P_O$ and 2P modes (or between the $2P_O$ and 2S modes), even when the amplitude and frequency are fixed. Our prior understanding of such $2P_O$ and 2P modes, which resemble (respectively) the 2P mode in the upper branch of free response (Govardhan and Williamson, 2000), and the 2P mode of the lower response branch, was that these patterns of vortex formation were simply the same 2P mode exhibiting somewhat different character in different parts of the 2P mode regime in the Williamson–Roshko map. However, it is significant that the 2P and $2P_O$ modes are distinct, both occurring at the same values of amplitude and wavelength. It was not possible to deduce this fact, based only on free vibration, because the higher fluid excitation ($C_Y \sin\phi$) of the $2P_O$ mode would necessarily push the vibration to higher amplitudes than the 2P mode. An understanding of this overlap regime is significant because it represents a region of positive fluid excitation that has the highest amplitude, and is responsible for exhibiting the peak amplitudes possible in free vibration.

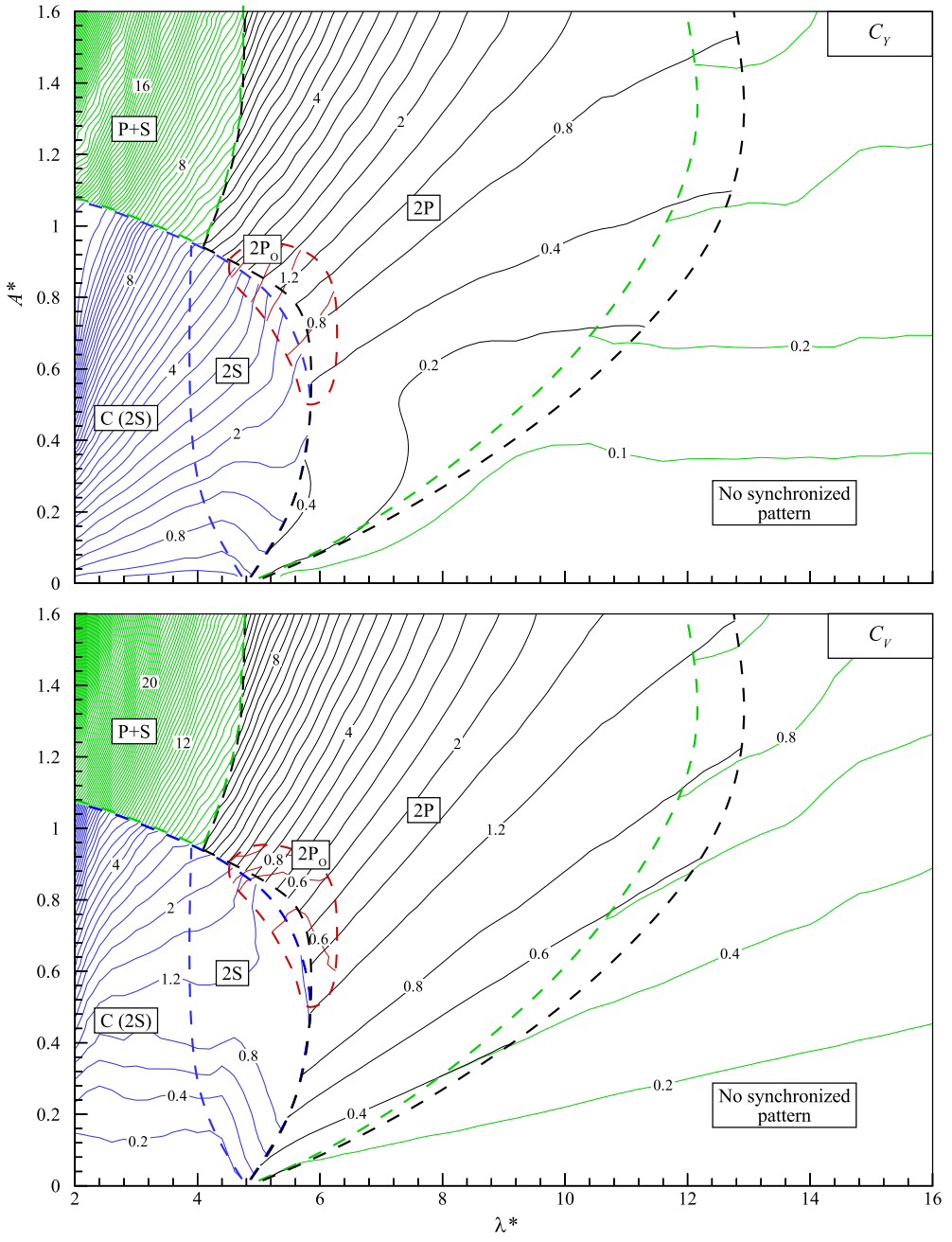

Fig. 13. Contours of the magnitude of the total force, C_Y, and the vortex force, C_V. Boundaries between modes are indicated by dashed lines. Contour interval in both cases is 0.4 with additional contours for very low forcing.

In this study, we also characterize the transitions across boundaries of the flow regimes within the amplitude–wavelength plane, illustrating the sometimes large changes in fluid force or vortex dynamics that can occur for small increments of amplitude or frequency of the controlled motion. Finally, we find that even in the desynchronized regime, where the vortex formation frequency becomes uncoupled to the body vibration frequency, the body *may be able to vibrate* due to the existence of a component of fluid forcing at the body vibration frequency, yielding positive fluid excitation. This is interesting, as most of the fluid force is associated with the uncoupled (and higher) vortex formation frequency, yet the wake is sufficiently organized by the body motion in a manner to yield

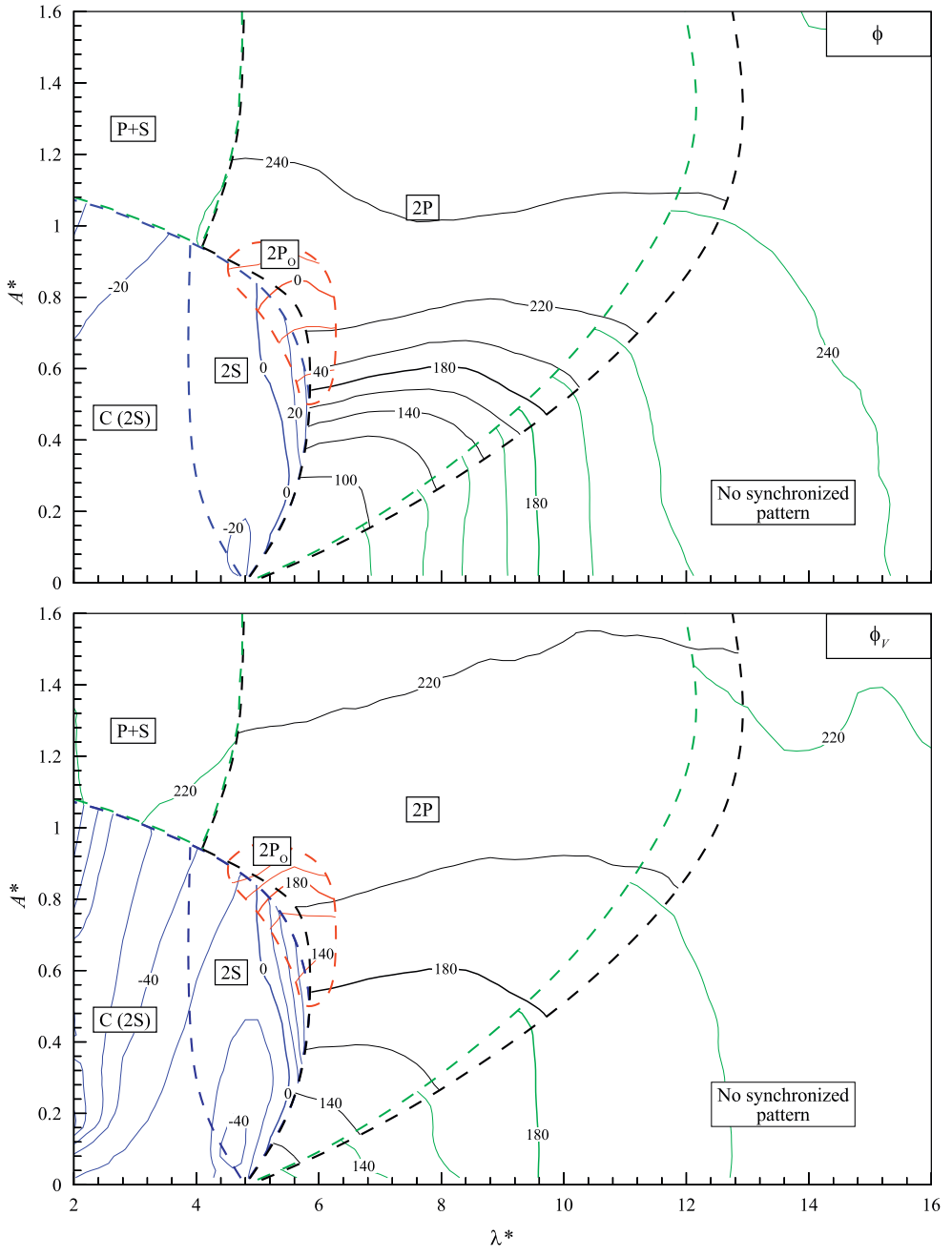

Fig. 14. Contours of the total phase, ϕ, and the vortex phase, ϕ_V. Boundaries between modes are indicated by dashed lines. Contour interval in both cases is 20°.

at least some positive fluid excitation. One might perhaps expect free vibration to exhibit a quasi-periodic response under these conditions.

Acknowledgments

The support from the Ocean Engineering Division of ONR, monitored by Dr Tom Swean, is gratefully acknowledged (ONR Contract Nos. N00014-04-1-0031 and N00014-07-1-0303). The authors would also like to thank Matt Horowitz and Raghu Govardhan for their enthusiastic and helpful input to this research.

Appendix A. Additional fluid forcing contours

In Section 3 we showed contours of $C_Y \sin\phi$ and $C_Y \cos\phi$. Here we present contour plots of the total force, C_Y, and vortex force C_V, in Fig. 13, as well as the total phase, ϕ, and vortex phase, ϕ_V, in Fig. 14. The different regimes of vortex shedding are perhaps most easily characterized by the phase angle in Fig. 14. When transitioning from the 2S mode to the $2P_O$ mode, there is no strong jump in total phase, however there is a large jump of about 180° in the vortex phase. When transitioning from the $2P_O$ mode to the 2P mode, the large jump occurs in the total phase, with only a small change in the vortex phase (since the basic vortex shedding mode is not varying).

References

Bearman, P.W., 1984. Vortex shedding from oscillating bluff bodies. Annual Review of Fluid Mechanics 16, 195–222.
Bishop, R.E.D., Hassan, A.Y., 1964. The lift and drag forces on a circular cylinder oscillating in a flowing fluid. Proceedings of the Royal Society London A 227, 51–75.
Carberry, J., Govardhan, R., Sheridan, J., Rockwell, D., Williamson, C.H.K., 2004. Wake states and response branches of forced and freely oscillating cylinders. European Journal of Mechanics B—Fluids 23, 89–97.
Carberry, J., Sheridan, J., Rockwell, D., 2001. Forces and wake modes of an oscillating cylinder. Journal of Fluids and Structures 15, 523–532.
Carberry, J., Sheridan, J., Rockwell, D., 2003. Controlled oscillations of a cylinder: a new wake state. Journal of Fluids and Structures 17, 337–343.
Carberry, J., Sheridan, J., Rockwell, D., 2005. Controlled oscillations of a cylinder: forces and wake modes. Journal of Fluid Mechanics 538, 31–89.
Feng, C.C., 1968. The measurement of vortex-induced effects in flow past stationary and oscillating circular and D-section cylinders. Master's Thesis, University of British Columbia, Vancouver, BC, Canada.
Gopalkrishnan, R., 1993. Vortex-induced forces on oscillating bluff cylinders. Ph.D. Thesis, MIT, Cambridge, MA, USA.
Govardhan, R., Williamson, C.H.K., 2000. Modes of vortex formation and frequency response of a freely vibrating cylinder. Journal of Fluid Mechanics 420, 85–130.
Govardhan, R., Williamson, C.H.K., 2006. Defining the 'modified Griffin plot' in vortex-induced vibration: revealing the effect of Reynolds number using controlled damping. Journal of Fluid Mechanics 561, 147–180.
Griffin, O.M., Ramberg, S.E., 1982. Some recent studes of vortex shedding with application to marine tubulars and risers. ASME Journal of Energy Resources Technology 104, 2–13.
Gu, W., Chyu, C., Rockwell, D., 1994. iming of vortex formation from an oscillating cylinder. Physics of Fluids 6, 3677–3682.
Hover, F.S., Techet, A.H., Triantafyllou, M.S., 1998. Forces on oscillating uniform and tapered cylinders in crossflow. Journal of Fluid Mechanics 363, 97–114.
Khalak, A., Williamson, C.H.K., 1996. Dynamics of a hydroelastic cylinder with very low mass and damping. Journal of Fluids and Structures 10, 455–472.
Mercier, J.A., 1973. Large amplitude oscillations of a circular cylinder in a low speed stream. Ph.D. Thesis, Stevens Institute of Technology, Hoboken, NJ, USA.
Morse, T.L., Williamson, C.H.K., 2006. Employing controlled vibrations to predict fluid forces on a cylinder undergoing vortex-induced vibration. Journal of Fluids and Structures 22, 877–884.
Morse, T.L., Williamson, C.H.K., 2009. Prediction of vortex-induced vibration response by employing controlled vibration. Journal of Fluid Mechanics, accepted for publication.
Ongoren, A., Rockwell, D., 1988a. Flow structure from an oscillating cylinder. Part 1. Mechanisms of phase shift and recovery in the near wake. Journal of Fluid Mechanics 191, 197–223.
Ongoren, A., Rockwell, D., 1988b. Flow structure from an oscillating cylinder. Part 2. Mode competition in the near wake. Journal of Fluid Mechanics 191, 225–245.
Parkinson, G., 1989. Phenomena and modelling of flow-induced vibrations of bluff bodies. Progress in Aerospace Science 26, 169–224.
Pottebaum, T.S., 2003. The relationship between near-wake structure and heat transfer for an oscillating circular cylinder in cross-flow. Ph.D. Thesis, Caltech, Pasadena, CA, USA.
Sarpkaya, T., 1977. Transverse oscillations of a circular cylinder in uniform flow, Part I. Tech. Rep. NPS-69SL77071, Naval Postgraduade School, Monterey, CA, USA.
Sarpkaya, T., 1979. Vortex-induced oscillations. ASME: Journal of Applied Mechanics 46, 241–258.
Staubli, T., 1983. Calculation of the vibration of an elastically mounted cylinder using experimental data from forced vibration. ASME: Journal of Fluids Engineering 105, 225–229.
Williamson, C.H.K., Govardhan, R., 2004. Vortex-induced vibrations. Annual Review of Fluid Mechanics 36, 413–455.
Williamson, C.H.K., Roshko, A., 1988. Vortex formation in the wake of an oscillating cylinder. Journal of Fluids and Structures 2, 355–381.